

Higher order organizational features can distinguish protein interaction networks of disease classes: a case study of neoplasms and neurological diseases

Vikram Singh,^{1†} Vikram Singh,^{1*}

¹Centre for Computational Biology and Bioinformatics, Central University of Himachal Pradesh, Dharamshala, Himachal Pradesh, 176206, India

*To whom correspondence should be addressed; E-mail: vikramsingh@cuhimachal.ac.in

Neoplasms (NPs) and neurological diseases and disorders (NDDs) are amongst the major classes of diseases underlying deaths of a disproportionate number of people worldwide. To determine if there exist some distinctive features in the local wiring patterns of protein interactions emerging at the onset of a disease belonging to either of these two classes, we examined 112 and 175 protein interaction networks belonging to NPs and NDDs, respectively. Orbit usage profiles (OUPs) for each of these networks were enumerated by investigating the networks' local topology. 56 non-redundant OUPs (nrOUPs) were derived and used as network features for classification between these two disease classes. Four machine learning classifiers, namely, k-nearest neighbour (KNN), support vector machine (SVM), deep neural network (DNN), random forest (RF) were trained on these data. DNN obtained the greatest average AUPRC (0.988) among these classifiers. DNNs developed on node2vec and the proposed nrOUPs embeddings were compared using 5-fold cross valida-

tion on the basis of average values of the six of performance measures, viz., AUPRC, Accuracy, Sensitivity, Specificity, Precision and MCC. It was found that nrOUPs based classifier performed better in all of these six performance measures.

1 Introduction

Understanding complex human diseases require linking disease phenotypes to their underlying molecular mechanisms and genetic components (1). With the advent of the biological big-data age, characterising the molecular or genetic elements of diseases has become equally crucial as characterising them based on their pathological and clinical manifestations (2). Next-generation sequencing (NGS) and genome-wide association studies (GWAS) have facilitated the collection of many disease-gene associations (3). Parallely, extensive protein interaction maps have been constructed due to recent advances in high-throughput proteomic technologies (4). An organism's genes are involved in several vital functions, including regulating cellular processes. The complex disease phenotypes of living beings arise due to the disintegration of the functional connections between genes that are intricately strung together (5). Since then, researchers in the biological sciences have used a wide range of experimental and computational methods to define the relationships between genes and the proteins they produce. Extensive population studies are being conducted to identify the genes implicated in common, multifactorial diseases and link the molecular pathology of simple monogenic disorders to their related clinical manifestations (6). The explanation of monogenic Mendelian inheritance patterns may aid the identification of pathogenic processes in complicated diseases. It is common for numerous genes to be involved in a complex disease, but pinpointing the exact genes responsible has proven difficult. The importance of understanding phenotype-genotype correlations in devising approaches to gene therapy is highlighted by the need for increased clinical research involving

vast numbers of patients.

Network medicine is a new discipline that uses network science methods to extract meaning from massive omics datasets on molecular diseases. The development of genotype-based disease networks was an early attempt to investigate the systemic significance of disease-gene associations from a network perspective (5). These networks are valuable for illuminating the global organisation of diseases around functional modules and for deducing comorbidity relations between diseases (7). Many subsequent studies have sought to expand upon the foundation laid by these early works by examining links between diseases (8,9). For instance, random walk algorithm has been exploited to discover previously unknown associations between diseases in the protein-protein interaction network (10). Similarly, differential coexpression analysis has been used to determine the degree of similarity between diseases and to reveal their shared molecular mechanisms, resulting in the discovery of novel interactions between diseases with previously unknown molecular mechanisms (11).

It has recently been established that the molecular architecture of human disease is modular (12). Several genetic diseases are traced back to changes in genes that are all part of the same cellular pathway, molecular complex, or functional module, lending credence to this line of thinking (13). It has been demonstrated, for instance, that proteins encoded by genes linked to the same disease are more likely to interact with one another than with proteins from other diseases (14). Moreover, in recent years a large volume of research has been focused on quantifying the similarities and differences among different disease classes using various similarity measures ranging from text mining to network topology. Various methods have been used to explore the connections between diseases. The most trustworthy approaches to identifying causal relationships between genes and diseases are genome-wide association studies (GWAS). Using GWAS data, researchers in several studies uncovered previously unknown connections between seemingly unrelated disorders (15). Comparing disease ontology (DO) and gene ontology (GO)

trees for semantic overlap is another method that has been exploited for the same (16). Moreover, these network-based methods have been used to study disease comorbidity and infer novel disease-associated genes.

Cancer and nervous system diseases are two critical issues in public health and are responsible for a significant number of deaths all around the globe. Cancer is a complicated, polygenic disorder that results from mutations in many genes (17). Contrarily, some brain diseases have monogenic roots, and others are polygenic (18). Rapid advances in high throughput approaches for generating biological data have made it possible to use a systems-level, integrative approach to study complex diseases (19, 20). In this study, we attempt to characterise the higher-order organisational patterns underlying 220 protein interaction networks belonging to these two classes of diseases and use these patterns to classify different networks into their respective classes.

2 Methods

2.1 Data acquisition and disease network construction

DisGeNET maintains one of the most extensive collections of genes associated with various monogenic, polygenic, rare diseases (related) and environmental traits (21). It combines data from various resources, including manually curated databases, text mining, GWAS datasets, and animal models, into one resource. The most authoritative disease-gene associations, *i.e.* those with GDA scores greater than 0.1, for neoplasm (MeSH class C04), nervous system diseases (C10), and two classes of psychiatry and psychology (F) MeSH superclass; including behavior and behavior mechanisms (F01), mental disorders (F03) were obtained from DisGeNET. Recent research from the Pan-Cancer Initiative (22) have shown that tumours of various organs share molecular features, while tumours of the same tissue may have vastly distinct genetic features. Motivated with these results, we combined all the types of neoplasms in one group and combined C10, F01, and F03 in one group called the neurological diseases and disorders (NDDs).

This grouping resulted in 331 diseases, 112 in the neoplasms (NPs) class and 219 in the NDDs class, associated with 10,880 unique genes. These 10,880 unique entrez gene ids belonging to the two disease classes were then mapped using UniPro Id mapper to identify their corresponding STRING ids. We could map 10,624 gene ids, so we discarded the unmapped 256 gene ids. Moreover, the diseases with less than 100 associated genes were also discarded. Out of 219 networks belonging to NDDs, we were able to map at least 100 entrez gene ids to matching STRING ids for 175 networks. However, this was not the case for the neoplastic networks, each of which contains at least 100 matching STRING ids. Thus this brings down the total number of networks utilised throughout the study to 257. To reconstruct a PPI network, we used human protein-protein interaction (PPI) information from the STRING database version 11.5 (23). STRING includes both experimentally verified and computationally inferred PPIs, along with an associated confidence score for each physical and functional interaction. We constructed the human contact network by selecting only interactions with confidence scores of 700 or higher to ensure we got only trustworthy interactions. Then the largest connected PIN component was obtained, containing 252,833 connections among 16,584 proteins.

2.2 Differentially expressed orbits (DEOs) identification

To construct random ensembles, we followed the same methodology explained in Singh et al. (24). Two types of random networks, Erdos Renyi and density dependent scale free models, were used to construct random ensembles corresponding to each disease network. Then orbit degree vector matrices for every network were obtained using the orbit counting algorithm (ORCA), which were further normalised to get orbit usage profiles (OUPs). Similarly, OUPs for both random ensembles were also enumerated, which were then compared with OUPs of disease networks to identify differentially expressed orbits (for complete methodology, please refer to Singh et al. (24)).

2.3 Preprocessing and classification of diseases

Before being used for training classification models, all OUP vectors were subjected to removal of 17 redundant orbits (25) and then each non-redundant OUP was appropriately normalised with min-max scaling. Formally, we used the following equation to normalise each N-dimensional feature vector x :

$$\hat{x} = \frac{x - \min(x)}{\max(x) - \min(x)}$$

, ensuring $0 \leq \hat{x} \leq 1 \forall i = 1, \dots, N$, where N denotes OUP's dimensions. We trained the support vector machine (SVM), naïve Bayes (NB), K-nearest neighbour (KNN), random forest (RF), and multi-layered deep neural network (DNN) supervised machine learning algorithms on the normalized OUPs to classify them. Classification with SVM involves kernel tricks, which include mapping a lower-dimensional space to a higher-dimensional one. To enhance prediction performance, we opted for the radial basis function (RBF) kernel and tuned two additional parameters, kernel width (γ) and regularisation C , between the ranges $2^{-5} - 2^{11}$ and $2^{-13} - 2^3$ respectively. The NB uses Bayes' theorem with the assumption that all possible feature pairs are uncorrelated with one another. Gaussian NB was used to construct the model for this investigation. In order to produce a prediction, KNN uses the geometric distance information of neighbours, which is a non-parametric technique. We choose five neighbours for this example. Random Forest (RF) is an ensemble method that constructs several decision trees by randomly sampling subspaces of feature vectors to make predictions. DNN implements one or more hidden layers (nonlinear approximators) between the input and output layers to make the classification. We have optimized the number of hidden layers, the number of units per layer, L2 regularization and solver parameters for DNN.

2.4 Performance evaluation

Five-fold cross-validation was used to compare the accuracy with which various classifiers predicted the training data. To ensure the predictors are reliable, randomly dividing the data into training and test sets, followed by model construction and evaluation, is performed a thousand times. Finally, the accuracy of the predictions was measured by four metrics: recall, specificity, accuracy, and Mathew correlation coefficient (MCC) which are defined as follows:

$$\begin{aligned} \textit{precision} &= \frac{TP}{TP + FP} \\ \textit{Recall} &= \frac{TP}{TP + FN} \\ \textit{Specificity} &= \frac{TN}{TN + FP} \\ \textit{MCC} &= \frac{TP \times TN - FP \times FN}{\sqrt{(TP + FP) \times (TP + FN) \times (TN + FP) \times (TN + FN)}} \end{aligned}$$

where TP, TN, FP, and FN represent true positive, true negative, false positive and false negative protein pairs. Furthermore, this represents a binary classifier with unbalanced positive and negative data sets, so precision-recall curves were used, and the area under the precision-recall curve (AUPRC) was computed (26).

3 Results and Discussion

In this section, we provide the results obtained and accompanying discussion by employing the aforementioned graphlet orbits-based methodology, first with regards to the study of differentially expressed orbits (DEOs) and subsequently with regards to the classification of non-redundant OUPs by means of several classification models.

3.1 Orbit enrichment and differential orbit expression analysis

As mentioned before, the OUPs of disease networks were compared to the OUPs of two different kinds of random network ensembles. In the end, this leads to a matrix of networks with significantly overexpressed orbits. To illustrate, in the Figure 1, we see the result of thresholding (Z -score) the differentially expressed orbit matrix ($DEOM$) at Z -score 2.58 or higher, i.e., keeping only the entries with Z -score more than or equal to 2.58 and setting the others to zero. The corresponding output table is shown in Table S of the supplementary materials. Only orbit 54 is disproportionately represented in networks for neoplastic diseases, while orbits 54 and 55 are disproportionately represented in networks for NDDs. Differentially expressed orbits of these two classes are identical because they are equivalence groups of the same graphlet G_{22} , which we refer to as a chevron.



Figure 1: Differentially expressed orbits (DEO): statistically significant orbits found to have Z -score > 2.58 for at least 50% networks of the same disease class.

Table 1: Prediction performance of DNN on nrOUP features of two disease classes

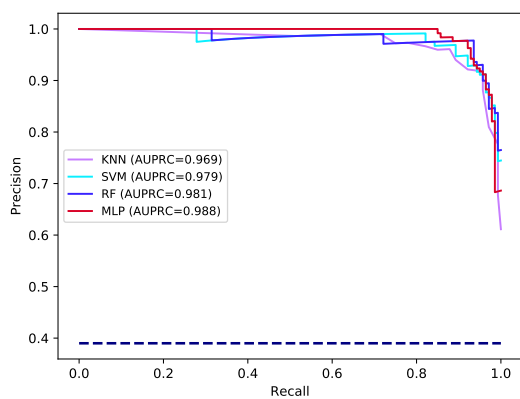
Fold#	AUPRC	Accuracy	Sensitivity	Speticity	Precision	MCC
0	1.0000	0.9348	1.0000	0.8333	0.9032	0.8676
1	0.9921	0.8696	0.8214	0.9444	0.9583	0.7483
2	0.9893	0.9130	0.8929	0.9444	0.9615	0.8243
3	0.9925	0.9565	1.0000	0.8889	0.9333	0.9108
4	0.9879	0.9111	0.8571	1.0000	1.0000	0.8330
Average (Std)	0.9923 (0.0047)	0.9170 (0.0323)	0.9143 (0.0822)	0.9222 (0.0633)	0.9513 (0.0359)	0.8368 (0.0601)

3.2 Performance of non-redundant OUP (nrOUPs) based DNN model

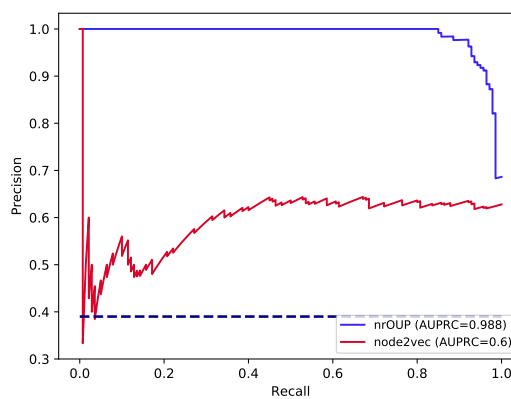
Our earlier work shows that the DNN outperforms other ML algorithms on a local topology-based measure called the orbit usage profile for distinguishing across classes of networks. As a result, we used the count of orbits in graphlets to encode each network as a 72-dimensional OUP vector, from which we removed the redundant orbits to obtain 56 non-redundant OUPs (nrOUPs). nrOUPs were classified using a deep multi-layered neural network (DNN), while model parameters, such as the number and size of hidden layers, regularisation, activation function, and solver, were optimised using a five-fold cross-validation approach. In particular, the best results are achieved using four hidden layers of 1000 units each, the relu activation function, and the adam solver. In the training set, we saw an average prediction accuracy of 97%, whereas, in the test set, it was only 97%. The experimental findings on the nrOUPs datasets are summarised in Table 1, where we see that the average accuracy of the fivefold CV technique is 91.7%, sensitivity is 91.43%, specificity is 92.22%, precision is 95.13%, the MCC is 83.6%, and the AUPRC value is 0.9923. Standard deviations for these performance measures are observed to be 3.23, 8.22, 6.33, 3.59, 6.01 and 0.0047, respectively. The lowest accuracy value recorded was 86.96% while the maximum accuracy value was up to 95.65% across all five sets of predicted performance. We employed DNNs to categorise DEOs and compared the results to other popular classifier models. In particular, we optimised the hyperparameters of KNN, RF, and SVM models using five-fold cross-validation and trained them on the same nrOUPs features used to train DNN. Table 2 summarises the experimental findings achieved by various classifiers on the nrOUPs dataset. Table 2 shows that, compared to previous classifier models, the proposed model using the DNN as the classifier achieved much higher accuracy and AUPRC values (Figure 2a). Accuracy-wise, RF and DNN classifiers are on par; however, AUPRC for DNN is marginally superior to the RF classifier.

Table 2: Prediction performance of different classifiers on nrOUP features of two disease classes

Classifier	AUPRC		Accuracy		Sensitivity		Specificity		Precision		MCC	
	Average	Std	Average	Std	Average	Std	Average	Std	Average	Std	Average	Std
KNN	0.9793	0.0184	0.9039	0.0199	0.8786	0.0479	0.9444	0.068	0.9639	0.0423	0.811	0.0392
SVM	0.9833	0.0144	0.9216	0.0499	0.9429	0.0407	0.8889	0.0878	0.9312	0.0533	0.8361	0.1062
DNN	0.9914	0.0049	0.9344	0.0161	0.95	0.0598	0.9111	0.0745	0.9467	0.0424	0.8684	0.0269
RF	0.9842	0.0138	0.9388	0.0099	0.9357	0.0466	0.9444	0.0556	0.9655	0.0339	0.877	0.0195



(a)



(b)

Figure 2: Performance of various classifiers for their ability to predict disease networks (a). The deep neural network (DNN) model beat the K-nearest neighbour (KNN), support vector machine (SVM), and random forest (RF) classifiers on the independent test set, as measured by the areas under the PrecisionRecall curves (AUPRC). (b) How well nrOUP and node2vec, two separate node embedding techniques, perform in DNN classifiers. According to the AUPRC, the nrOUP technique is superior to the node2vec encoding scheme.

3.3 Performance of nrOUP against node2vec embedding

Each network was transformed into a 66-dimensional vector representation, much like nrOUPs, by first generating a 12-dimensional vector representation via the node2vec technique. Here, we specify values 4, 10, and 12 for three hyperparameters, defining the walk length per source, the number of walks per source, and the output dimensions. We then employed cosine similarity to transform the data from each dimension into a (12, 12) matrix. Then, we took the lower triangular half of the similarity matrix (66 dimensions in total) and utilised it as a feature vector to characterise the whole network. Table 3 displays the results of a classification exercise utilising DNN and node2vec embeddings. Compared to nrOUPs, the AUPRC obtained utilising node2vec features is extremely low, only 0.6 (Figure 2b). Moreover, nrOUPs improved upon all of the six performance evaluation metrics shown in Table 3 compared to node2vec embeddings. We further generated confusion matrices for both nrOUP and node2vec features. Only nine per cent of the NP networks were misclassified into NDD networks when we used nrOUP features (Figure 3a). On the other hand, 61% of neoplastic networks were predicted as neurological networks, and 23% of neurological networks were misclassified as neoplastic networks (Figure 3b).

Table 3: Prediction performance of DNN on nrOUP and ndoe2vec features of two disease classes

Features	AUPRC		Accuracy		Sensitivity		Sppecificity		Precision		MCC	
	Average	Std	Average	Std	Average	Std	Average	Std	Average	Std	Average	Std
nrOUP	0.9919	0.0048	0.9257	0.0251	0.9286	0.0714	0.9222	0.0843	0.9533	0.0485	0.8535	0.0478
Node2vec	0.6499	0.1239	0.5722	0.0576	0.6786	0.0253	0.4052	0.1706	0.6484	0.0677	0.0814	0.154

4 Summary and Conclusions

Cancer and other brain-related disorders account for a disproportionate share of all disease-related deaths. In a recent study called the Pan-Cancer Initiative, researchers found that while

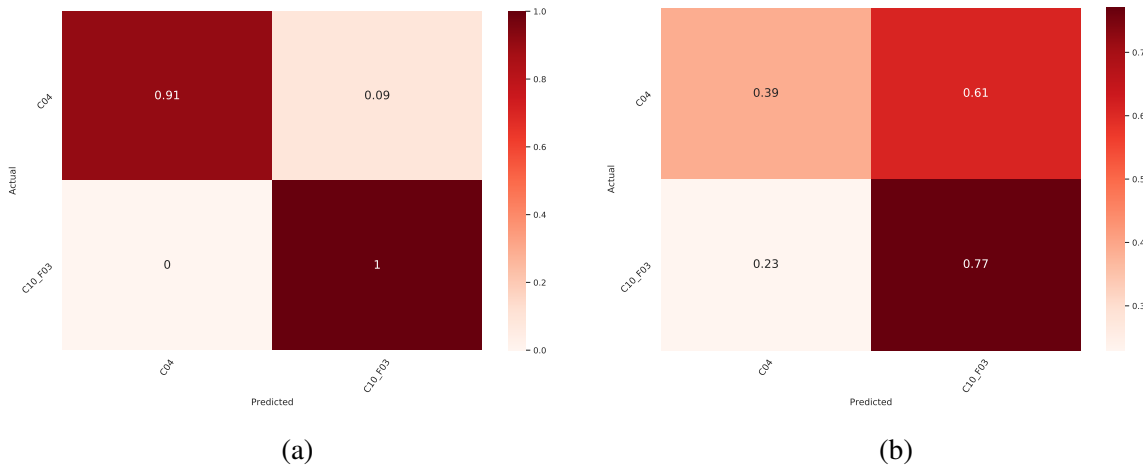


Figure 3: Confusion matrices representing the performance of DNN on nrOUP (a) and node2vec (b) features.

tumours in the same tissue can have widely different genetic traits, tumours in other organs share common molecular features. Those findings prompted us to question whether or not we could use network-level similarities and differences to categorise diseases into their respective classes. As part of our research, we built 287 networks for two types of diseases: tumours (112) and neurological disorders (175). The networks' local architectures were then investigated to collect individual profiles of orbital usage called OUPs. Orbit 54 was shown to be differentially expressed in neoplastic networks, while orbits 54 and 55 were found to be differentially expressed in brain illness networks. Following this, 56 unique OUPs were extracted from the OUPs and used as features for disease network classification. After training four classifiers (KNN, SVM, RF, and DNN) with nrOUPs, DNN proved to be the most effective and had the highest average AUPRC of 0.988. Finally, we evaluated the performance of DNN on nrOUPs and node2vec embeddings and found that nrOUP performed better than node2vec in all the six performance evaluation metrics used in this study.

References

1. D. Weatherall, *Nature reviews genetics* **2**, 245 (2001).
2. M. Oti, M. A. Huynen, H. G. Brunner, *Trends in genetics* **24**, 103 (2008).
3. V. Tam, *et al.*, *Nature Reviews Genetics* **20**, 467 (2019).
4. *Nucleic acids research* **49**, D480 (2021).
5. A.-L. Barabási, N. Gulbahce, J. Loscalzo, *Nature reviews genetics* **12**, 56 (2011).
6. L. T. Elliott, *et al.*, *Nature* **562**, 210 (2018).
7. J. X. Hu, C. E. Thomas, S. Brunak, *Nature Reviews Genetics* **17**, 615 (2016).
8. K.-I. Goh, I.-G. Choi, *Briefings in functional genomics* **11**, 533 (2012).
9. J. Xiang, J. Zhang, Y. Zhao, F.-X. Wu, M. Li, *Briefings in Bioinformatics* **23**, bbac006 (2022).
10. A. Suratane, K. Plaimas, *Bioinformatics and Biology insights* **9**, BBI (2015).
11. J. Yang, S.-J. Wu, W.-T. Dai, Y.-X. Li, Y.-Y. Li, *Biology direct* **10**, 1 (2015).
12. M. Oti, H. G. Brunner, *Clinical genetics* **71**, 1 (2007).
13. H. Joenje, K. J. Patel, *Nature Reviews Genetics* **2**, 446 (2001).
14. K.-I. Goh, *et al.*, *Proceedings of the National Academy of Sciences* **104**, 8685 (2007).
15. W. Huang, P. Wang, Z. Liu, L. Zhang, *BMC bioinformatics* **10**, 1 (2009).
16. S. Mathur, D. Dinakarpanian, *Journal of biomedical informatics* **45**, 363 (2012).

17. D. Hanahan, *Cancer discovery* **12**, 31 (2022).
18. S. A. McCarroll, S. E. Hyman, *Neuron* **80**, 578 (2013).
19. G. Kar, A. Gurosoy, O. Keskin, *PLoS computational biology* **5**, e1000601 (2009).
20. J. A. Santiago, J. A. Potashkin, *Trends in molecular medicine* **20**, 694 (2014).
21. J. Piñero, *et al.*, *Nucleic acids research* **48**, D845 (2020).
22. J. N. Weinstein, *et al.*, *Nature genetics* **45**, 1113 (2013).
23. D. Szklarczyk, *et al.*, *Nucleic acids research* **49**, D605 (2021).
24. V. Singh, V. Singh, *arXiv preprint arXiv:2203.00999* (2022).
25. Ö. N. Yaveroğlu, *et al.*, *Scientific reports* **4**, 1 (2014).
26. J. Davis, M. Goadrich, *Proceedings of the 23rd international conference on Machine learning* (2006), pp. 233–240.

ACKNOWLEDGEMENTS

VS[†] thanks Council of Scientific and Industrial Research (CSIR), India for providing Junior Research Fellowship (JRF). **Funding:** Authors received no specific funding for this research work. **Authors Contributions:** VS* conceptualized and designed the research framework. VS[†] performed the computational experiments. VS[†] and VS* analyzed the data and interpreted results. VS[†] and VS* wrote and finalized the manuscript. **Competing Interests:** The authors declare that they have no conflict of interests. **Data and materials availability:**